ISBN: 978-3-95450-132-8 doi:10.18429/JACoW-IPAC2014-WEPRO073

THE ESS HIGH ENERGY BEAM TRANSPORT AFTER THE 2013 DESIGN UPDATE

H.D. Thomsen*, S.P. Møller, ISA, Aarhus University, 8000 Aarhus C, Denmark

Abstract

Following an optimization of the European Spallation Source (ESS) linac, a number of changes have been introduced in the High Energy Beam Transport (HEBT). In particular, about 120 m of beam transport has been allocated to enable an extension of the superconducting linac, thus providing some contingency against poor linac performance and potentially allowing a future beam power upgrade. The changes in layout and beam optics in all HEBT lines will be discussed.

INTRODUCTION

The year 2013 has brought many changes to the ESS accelerator, even top level beam parameters, while maintaining the average beam power of 5 MW [1]. Indirectly due to the increase in peak beam current to 62.5 mA (to compensate for a reduction in beam energy to 2.0 GeV), the concept for expanding the beam on the target surface (the beam entrance window, BEW) has been revisited and changed [2]. Although many requirements remain similar, the changes have required an overhaul of the beam optics of the ESS HEBT. Especially the contingency region and the vertical dogleg have been changed considerably in this process.

BEAM OPTICS

The primary line in the HEBT brings the beam from the accelerator to the target, while leaving room for accelerator upgrades, overcoming an 4.5 m elevation, and setting the transverse profiles on the target. These requirements are met through three separate sections with appropriate matching flexibility in-between. A sketch of the mechanical layout can be seen in Fig. 1. The lattice and beam optics of the HEBT can be seen in Fig. 2. The purpose and optics of the principal sections will be discussed in the following.

Upgrade High-β (UHB)

The UHB provides contingency in the linac performance through the possibility to extend the High-β (Hβ) linac into this region. The UHB consists of 15×8520 mm Hβ periods, of which one is reserved for a differential pumping stage. Nominally, the periods will only consist of a quadrupole doublet unit (providing transverse focusing, dipole corrections, beam instrumentation, and vacuum equipment) and a 6587.6 mm spool pipe piece as a substitute for a cryomodule. Figure 2 reveals a subdivision of the UHB. The first 4 doublet periods are used to match the linac beam, cf. Table 1, to a section consisting of 6 periods with a transverse phase advance of 30° per period. The latter section includes a transverse movable collimator system consisting of three identical collimator stations, located 60° apart for a hexagonal coverage in the transverse normalized phase spaces.

Table 1: Assumed HEBT Input Beam Twiss Parameters, Courtesy of M. Eshraqi, ESS

	Unit	$w = x$	$w = y$	$w = z$
α_w	—	−1.728	0.165	0.153
β_w	mm/π.mrad	55.08	41.11	54.51
$\epsilon_{n.w}$	π.mm.mrad	0.344	0.359	0.395

Figure 1: A sketch of the HEBT layout.

The final part of the UHB is essentially a long matching section, steadily ramping the vertical phase advance per cell up to the larger value necessary in the achromatic dogleg.

Dogleg

Compared to previous layouts, the vertical dogleg is now longer and more shallow with an angle of only 4°. The reduced angle can feasibly be introduced by only a single 1.8 m dipole at either end of the dogleg. Preliminary evaluation of the dipole design indicates that the horizontal gap can be increased, such that it should be possible to maintain the same minimum physical beam tube aperture throughout the UHB and dogleg. The smaller angle also facilitates a simpler building design, essentially now a sloped tunnel, reducing the construction cost considerably. With the reduction of the angle, the separation between the dogleg line and the straight-ahead tuning dump line takes place over a longer distance. Clearance between the dump line beam tube and the first dogleg quadrupole yoke calls for a longer period length of 10.752 m in the dogleg.

Between the dipole centres, 6 identical quadrupole doublet periods provide the necessary vertical phase advance of $6 \times 60°$, thus cancelling the vertical dispersion to first order. This will limit dispersive effects at the target and the general impact of linac RF failures, as discussed elsewhere [3]. As in the UHB, all quadrupoles of the dogleg have auxiliary coils to introduce a dipole corrector field acting in the focusing plane.

Accelerator to Target (A2T)

As described in [2, 4] the idea of using non-linear magnets to deliver more flat beam profiles to the target [5] has been abandoned due to its sensitivity to the characteristics

* heinetho@phys.au.dk

ISBN: 978-3-95450-132-8 doi:10.18429/JACoW-IPAC2014-WEPRO073

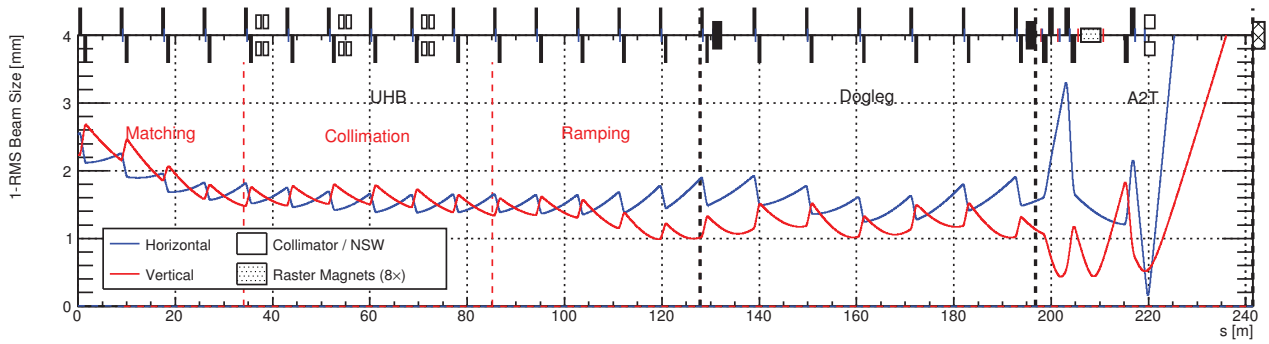

Figure 2: The 1-RMS transverse optics leading the beam from the accelerator interface (s = 0 m) to the target surface (s = 241.4 m). The lattice is shown above, using standard symbols for quadrupoles and dipoles.

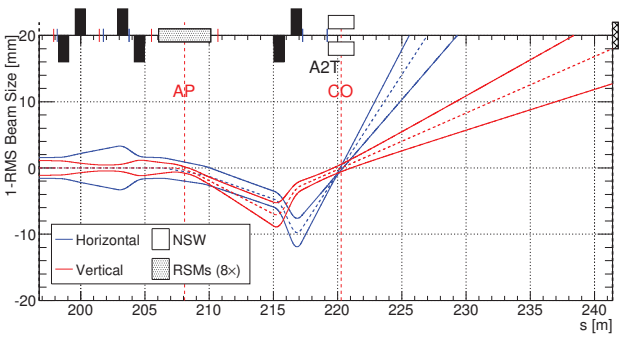

Figure 3: The 1-RMS transverse beam optics along the A2T at maximum raster amplitudes.

of the incoming beam, in particular the transverse kurtosis, *i.e.* halo. Instead, a linear raster system has been designed. based on ideas from similar systems for the LANL APT [6] and MTS [7]. This paper will describe the nominal beam optics and operation of the system and A2T in general. A more technical discussion of the raster scanning magnet (RSM) system is given in [8].

A set of 8 dithering RSM dipoles, 4 acting in each plane, introduces fast AC transverse beam centroid displacements at the target and proton beam window (PBW). Setting a sweep frequency ratio in the two planes, f_y/f_x, the RSMs produce a fine-meshed Lissajous-like pattern with an rectangular outline. Such an approach, combined with a $\simeq$ 0.84 cm^2 beamlet, generates a time-averaged intensity distribution with a large uniform central region and less than 1% beam deposited outside the 180×60 mm^2 nominal footprint. Beamlet sizes and displacement amplitudes can be seen in Table 2. A frequency ratio of $f_y/f_x = 113/83$ (possibly $f_x = 29$ kHz and $f_y = 40$ kHz) has been assumed for the simulations. The rastered distribution could benefit (in terms of reduced peak intensity and sharper edge) from reducing the beamlet dimensions. This would however increase the static beamlet power density, which could be harmful to the PBW and BEW in case of full failure of the raster system.

Besides Fig. 2, the A2T optics is also shown in Fig. 3. In Fig. 2 the beam is centered on the target (RSMs are off), while the latter picture represents a snapshot of the optics while the raster actions are at nominal amplitudes. The principle of the optics is described in detail elsewhere [2], but will be mentioned here briefly. The A2T DC elements comprises 6 identical quadrupoles. The final quadrupole doublet, downstream of the RSMs, impose a transverse phase advance of 180° between the common RSM action point (AP) and the beam crossover (CO). Assuming the nominal optics, the CO thus becomes a pivot point of the oscillating raster motion. The first 4 quadrupoles of the A2T constitute a matching section that provide a beam waist at the CO and set the beamlet dimensions on the target, cf. Table 2. Especially downstream of the CO, where the oscillating deflections become large, the raster system effectively increases the time-averaged transverse emittances of the linac beam (by more than an order of magnitude in the horizontal plane). At the CO, where the deflections are neutralized by design, the emittances are however unaffected by the RSM system. The CO is thus a suitable location for a small-aperture neutron shield wall (NSW) that limits the intensity of back-streaming neutrons while not intercepting the primary beam during operation. The NSW is modelled as a Ø40 mm × 2000 mm aperture around the CO beam waist.

Figure 3 also depicts the location of beam position monitors (blue lines) and four separate 2D dipole correctors (red lines). These units will correct the transverse beam displacement and angle before going through the RSM and CO apertures. Such DC correction procedures can advantageously be performed with a low-power (short-pulse) accelerator mode, while having the RSMs off.

Beam Dump Line (DMPL)

To tune up the accelerator and the UHB, a low-power beam can be disposed at a 12.5 kW tuning dump. Even at full energy and peak current, the beam power can be limited through the proton beam duty cycle, *i.e.* the proton pulse duration (Δt_p) and repetition rate. For 12.5 kW of average power, the duty cycle should be below 10^{-4}; possibly 1 Hz, $\Delta t_p = 100$ μs. Being in line of sight with the accelerator, this alternative beam destination is insensitive to changes in the beam energy and allows machine studies and tuning.

ISBN: 978-3-95450-132-8 doi:10.18429/JACoW-IPAC2014-WEPRO073

Table 2: Beam parameters, Horizontal (H) and Vertical (V)

Parameter	Location	H	V
RMS beam size	CO	0.32 mm	0.56 mm
	PBW	12.6 mm	4.24 mm
	BEW	15.9 mm	5.30 mm
Max. displacement	PBW	49.9 mm	14.3 mm
	BEW	63.0 mm	18.0 mm
Avg. current density	PBW	88 μA/cm^2	
	BEW	56 μA/cm^2	

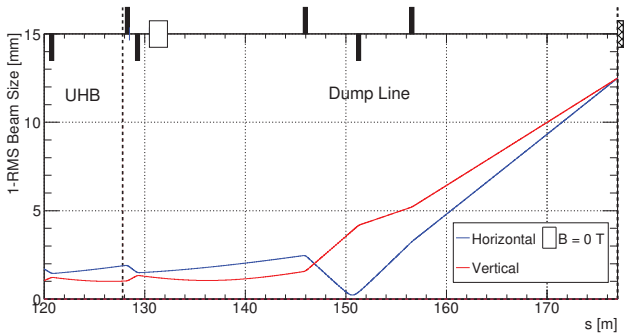

Figure 4: The 1-RMS transverse optics of the beam dump line with the dump located at the far right, s = 177 m.

The 1-RMS transverse optics along the beam dump line (DMPL) can be seen in Fig. 4. The final UHB quadrupoles, visible far upstream in the figure, are left at their nominal gradients, leaving the absent dipole field as the first difference from the nominal, full-power optics. The DMPL is based on a quadrupole triplet which sets a 12.5 mm RMS beam size in both transverse directions at the dump surface.

Preliminary estimates of the dogleg dipole magnetic design suggests a remanence field of the order of 0.4% of the nominal field. Besides the main unipolar supply, a complete neutralization of the field would require a bipolar corrector supply connected to auxiliary coils in the dipole. If uncompensated here or by downstream correctors, this error (corresponding to a 0.28 mrad angular error at the dipole) would lead to a 33 mm constant vertical beam centroid displacement at the dump.

BEAM LOSSES

To minimize the uncontrolled beam losses along the HEBT, the beam tube aperture is kept relatively large along the main line, leading the beam to the main target station, that should accept the full beam power and the associated losses. Except for at the NSW and the RSMs, the minimum physical inner tube diameter is 100 mm. The ratio of the beam tube bore radius and the 1-RMS beam size, the normalized beam aperture, can be seen in Fig. 5. In general, the normalized aperture is $\gtrsim$ 20 and does not go below 10 until reaching the target monolith (visible as a distinct kink in the vertical line near s = 235 m). The uncontrolled beam losses along the ESS HEBT are thus in general expected to be low. With the lower beam power, the beam dump line should allow for larger relative beam losses while still respecting the requirements for hands-on maintenance. Slightly lower normalized apertures should thus be acceptable in the DMPL.

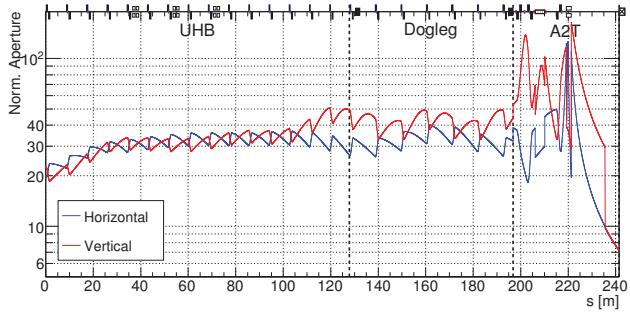

Figure 5: Normalized aperture along the HEBT with the beam sent to the nominal destination, the target station.

CONCLUSION

The optics of the ESS HEBT following a major revision has been presented. In general, the HEBT line can efficiently bring the beam from the linac to the target. The principal HEBT sections (UHB, dogleg, A2T) provide separate matching sections to control the transverse beam parameters, thus offering tuning flexibility towards deviations from nominal beam parameters. The sensitivity to non-nominal beam conditions and lattice imperfections is explored elsewhere [3].

Comparing the optics with the current assumptions on the vacuum apertures, the uncontrollable beam losses are expected to be low, as the normalized aperture is comparable or better than at similar facilities, like the SNS.

REFERENCES

[1] M. Eshraqi *et al.*, IPAC'14, THPME043 (2014).

[2] H.D. Thomsen *et al.*, IPAC'13, MOPEA005, p. 70 (2013).

[3] H.D. Thomsen *et al.*, IPAC'14, WEPRO074 (2014).

[4] T.J. Shea *et al.*, NA-PAC'13, MOPMA04 (2013).

[5] A.I.S. Holm *et al.*, IPAC'12, MOPPD049, p. 475 (2012).

[6] S. Chapelle *et al.*, LINAC'98, TU4089, p. 612 (1998).

[7] B. Blind *et al.*, LINAC 2006, MOP055, p. 171 (2006).

[8] H.D. Thomsen *et al.*, IPAC'14, WEPRO072 (2014).